ICHEP94 Ref. GSL0391 **CLEO CONF 94-3**
Submitted to PA 21,2 Pl 9,19 **July 18, 1994**

Search for Exclusive Charmless Hadronic B Decays

J. Gronberg,[1] R. Kutschke,[1] S. Menary,[1] R.J. Morrison,[1] S. Nakanishi,[1] H.N. Nelson,[1] T.K. Nelson,[1] C. Qiao,[1] J.D. Richman,[1] A. Ryd,[1] H. Tajima,[1] D. Sperka,[1] M.S. Witherell,[1] R. Balest,[2] K. Cho,[2] W.T. Ford,[2] D.R. Johnson,[2] K. Lingel,[2] M. Lohner,[2] P. Rankin,[2] J.G. Smith,[2] J.P. Alexander,[3] C. Bebek,[3] K. Berkelman,[3] K. Bloom,[3] T.E. Browder,[3*] D.G. Cassel,[3] H.A. Cho,[3] D.M. Coffman,[3] D.S. Crowcroft,[3] P.S. Drell,[3] D. Dumas,[3] R. Ehrlich,[3] P. Gaidarev,[3] M. Garcia-Sciveres,[3] B. Geiser,[3] B. Gittelman,[3] S.W. Gray,[3] D.L. Hartill,[3] B.K. Heltsley,[3] S. Henderson,[3] C.D. Jones,[3] S.L. Jones,[3] J. Kandaswamy,[3] N. Katayama,[3] P.C. Kim,[3] D.L. Kreinick,[3] G.S. Ludwig,[3] J. Masui,[3] J. Mevissen,[3] N.B. Mistry,[3] C.R. Ng,[3] E. Nordberg,[3] J.R. Patterson,[3] D. Peterson,[3] D. Riley,[3] S. Salman,[3] M. Sapper,[3] F. Würthwein,[3] P. Avery,[4] A. Freyberger,[4] J. Rodriguez,[4] S. Yang,[4] J. Yelton,[4] D. Cinabro,[5] T. Liu,[5] M. Saulnier,[5] R. Wilson,[5] H. Yamamoto,[5] T. Bergfeld,[6] B.I. Eisenstein,[6] G. Gollin,[6] B. Ong,[6] M. Palmer,[6] M. Selen,[6] J. J. Thaler,[6] K.W. Edwards,[7] M. Ogg,[7] A. Bellerive,[8] D.I. Britton,[8] E.R.F. Hyatt,[8] D.B. MacFarlane,[8] P.M. Patel,[8] B. Spaan,[8] A.J. Sadoff,[9] R. Ammar,[10] P. Baringer,[10] A. Bean,[10] D. Besson,[10] D. Coppage,[10] N. Copty,[10] R. Davis,[10] N. Hancock,[10] M. Kelly,[10] S. Kotov,[10] I. Kravchenko,[10] N. Kwak,[10] H. Lam,[10] Y. Kubota,[11] M. Lattery,[11] M. Momayezi,[11] J.K. Nelson,[11] S. Patton,[11] R. Poling,[11] V. Savinov,[11] S. Schrenk,[11] R. Wang,[11] M.S. Alam,[12] I.J. Kim,[12] Z. Ling,[12] A.H. Mahmood,[12] J.J. O'Neill,[12] H. Severini,[12] C.R. Sun,[12] F. Wappler,[12] G. Crawford,[13] C. M. Daubenmier,[13] R. Fulton,[13] D. Fujino,[13] K.K. Gan,[13] K. Honscheid,[13] H. Kagan,[13] R. Kass,[13] J. Lee,[13] R. Malchow,[13] Y. Skovpen,[13†] M. Sung,[13] C. White,[13] M.M. Zoeller,[13] F. Butler,[14] X. Fu,[14] B. Nemati,[14] W.R. Ross,[14] P. Skubic,[14] M. Wood,[14] M. Bishai,[15] J. Fast,[15] E. Gerndt,[15] R.L. McIlwain,[15] T. Miao,[15] D.H. Miller,[15] M. Modesitt,[15] D. Payne,[15] E.I. Shibata,[15] I.P.J. Shipsey,[15] P.N. Wang,[15] M. Battle,[16] J. Ernst,[16] L. Gibbons,[16] Y. Kwon,[16] S. Roberts,[16] E.H. Thorndike,[16] C.H. Wang,[16] J. Dominick,[17] M. Lambrecht,[17] S. Sanghera,[17] V. Shelkov,[17] T. Skwarnicki,[17] R. Stroynowski,[17] I. Volobouev,[17] G. Wei,[17] P. Zadorozhny,[17] M. Artuso,[18] M. Gao,[18] M. Goldberg,[18] D. He,[18] N. Horwitz,[18] R. Kennett,[18] R. Mountain,[18] G.C. Moneti,[18] F. Muheim,[18] Y. Mukhin,[18] S. Playfer,[18] Y. Rozen,[18] S. Stone,[18] X. Xing,[18] G. Zhu,[18] J. Bartelt,[19] S.E. Csorna,[19] Z. Egyed,[19] V. Jain,[19] D. Gibaut,[20] K. Kinoshita,[20] P. Pomianowski,[20] B. Barish,[21] M. Chadha,[21] S. Chan,[21] D.F. Cowen,[21] G. Eigen,[21] J.S. Miller,[21] C. O'Grady,[21] J. Urheim,[21] A.J. Weinstein,[21] M. Athanas,[22] W. Brower,[22] G. Masek,[22] and H.P. Paar[22]

(CLEO Collaboration)

[1]*University of California, Santa Barbara, California 93106*
[2]*University of Colorado, Boulder, Colorado 80309-0390*
[3]*Cornell University, Ithaca, New York 14853*
[4]*University of Florida, Gainesville, Florida 32611*
[5]*Harvard University, Cambridge, Massachusetts 02138*
[6]*University of Illinois, Champaign-Urbana, Illinois, 61801*
[7]*Carleton University, Ottawa, Ontario K1S 5B6 and the Institute of Particle Physics, Canada*
[8]*McGill University, Montréal, Québec H3A 2T8 and the Institute of Particle Physics, Canada*
[9]*Ithaca College, Ithaca, New York 14850*
[10]*University of Kansas, Lawrence, Kansas 66045*
[11]*University of Minnesota, Minneapolis, Minnesota 55455*
[12]*State University of New York at Albany, Albany, New York 12222*
[13]*Ohio State University, Columbus, Ohio, 43210*
[14]*University of Oklahoma, Norman, Oklahoma 73019*
[15]*Purdue University, West Lafayette, Indiana 47907*
[16]*University of Rochester, Rochester, New York 14627*
[17]*Southern Methodist University, Dallas, Texas 75275*
[18]*Syracuse University, Syracuse, New York 13244*
[19]*Vanderbilt University, Nashville, Tennessee 37235*
[20]*Virginia Polytechnic Institute and State University, Blacksburg, Virginia, 24061*
[21]*California Institute of Technology, Pasadena, California 91125*
[22]*University of California, San Diego, La Jolla, California 92093*

Abstract

We have searched for several two-body charmless hadronic decays of B mesons. These final states include $K\pi$ and $\pi\pi$ with both charged and neutral kaons and pions; $K^*\pi$, $K\rho$, and $\pi\rho$; and ϕX_s, where $X_s = K$, K^*, or ϕ. The data used in this analysis consist of 2.0 fb^{-1} taken on the $\Upsilon(4S)$ with the CLEO-II detector at the Cornell Electron Storage Ring (CESR). This data set includes 2.2 million $B\overline{B}$ pairs, allowing us to place upper limits on these branching ratios in the range from 10^{-4} to 10^{-5}.

---

[*]Permanent address: University of Hawaii at Manoa

[†]Permanent address: INP, Novosibirsk, Russia

I. INTRODUCTION

The decays of B-mesons to two charmless hadrons can proceed via a $b \to u$ tree-level spectator diagram (Figure 1a), or via a $b \to sg$ one-loop "penguin-diagram" (Figure 1b) and to a lesser extent, via the CKM-suppressed $b \to dg$ penguin diagram. Although rare decays can also proceed via $b \to u$ internal, color-suppressed diagrams (Figure 1c), $b \to u$ exchange diagrams (Figure 1d), annihilation diagrams (Figure 1e), or vertical W loop diagrams (Figure 1f), these contributions are expected to be negligible in most cases.

Decays such as $B^0 \to \pi^+\pi^-$ and $B^0 \to \pi^\pm\rho^\mp$ are expected to be dominated by the $b \to u$ spectator diagram, and measurements of their branching fractions can be used to extract a value for $|V_{ub}|$. The decay mode $B^0 \to \pi^+\pi^-$ can be used to measure CP violation in the B sector at both asymmetric B factories [1] and hadron colliders [2]. Since the $\pi^+\pi^-$ final state is a CP eigenstate, CP violation can arise from interference between the amplitude for direct decay and the amplitude for the process in which the B^0 first mixes into a $\overline{B}^0$ and then decays. Measurement of the time evolution of the rate asymmetry leads to a measurement of $\sin 2\alpha$, where α is one of the angles in the unitarity triangle. If the $B^0 \to \pi^+\pi^-$ decay has a non-negligible contribution from the $b \to dg$ penguin diagram, the CP violation caused by interference between the spectator and penguin contributions will contaminate the measurement of CP violation via mixing [3], an effect known as "penguin pollution." If this is the case, the penguin and spectator effects can be disentangled by also measuring the isospin-related states $B^0 \to \pi^0\pi^0$ and $B^\pm \to \pi^\pm\pi^0$ [4].

Decays such as $B^0 \to K^+\pi^-$ and $B^0 \to K^{*+}\pi^-$ are expected to be dominated by the $b \to sg$ penguin diagram, with a small contribution from a Cabibbo-suppressed $b \to u$ spectator diagram. Interference between the penguin and spectator amplitudes can give rise to direct CP violation, which will appear as a rate asymmetry for decays of B^0 and $\overline{B}^0$ mesons, but the presence of hadronic phases complicates the extraction of the CP violation parameters. Gronau, Rosner, and London have shown [5] that the phase angle γ can be extracted using precise time-integrated measurements of B^+ decays to $K^0\pi^+$, $K^+\pi^0$, and $\pi^+\pi^0$ and their charge conjugates. These could be made at either a symmetric or an asymmetric B factory (CESR, KEK, SLAC), but they will require excellent particle identification to distinguish between the $K\pi$ and $\pi\pi$ modes.

Decays such as $B \to K\phi$ and $B^+ \to K^0\pi^+$ cannot occur via a spectator diagram and are expected to be dominated by the penguin diagram. Measurement of these decays will give direct information on the strength of the penguin amplitude.

Recent observations of the sum of the two-body charmless hadronic decays $B^0 \to K^+\pi^-$and $\pi^+\pi^-$ [6] and of the electromagnetic penguin decay $B \to K^*(892)\gamma$ [7], indicate that we have reached the sensitivity required to observe such phenomena. The large data set and precision detector of the CLEO experiment allow us to probe branching fractions at the 10^{-4} to 10^{-5} level.

This paper reports preliminary results on the decays $B^+ \to K^0\pi^+$, $B^0 \to K^0\pi^0$, $B^+ \to \pi^+\pi^0$, $B^+ \to K^+\pi^0$, $B^0 \to \pi^0\pi^0$, $B \to K^*\pi$, $B \to K\rho$, $B \to \pi\rho$, and $B \to X_s\phi$. We place upper limits on these modes in the range 10^{-4} to 10^{-5}. We also include updated results on the decays $B^0 \to K^+\pi^-$, $B^0 \to \pi^+\pi^-$, and $B^0 \to K^+K^-$.

II. DATA SAMPLE AND EVENT SELECTION

The data set used in this analysis was collected with the CLEO-II detector [8] at the Cornell Electron Storage Ring (CESR). It consists of 2.0 fb^{-1} taken on the $\Upsilon(4S)$ (on-resonance) and 0.9 fb^{-1} taken at a center of mass energy $\sim$ 55 MeV below the $\Upsilon(4S)$ (off-resonance). The on-resonance sample contains 2.2 million $B\overline{B}$ pairs. The off-resonance sample, taken below the $B\overline{B}$ threshold, is used for continuum background estimates.

The momenta of charged particles are measured using a 6-layer straw tube chamber, a 10-layer precision drift chamber, and a 51-layer main drift chamber, all operating inside a 1.5-T superconducting solenoid. The main drift chamber also provides a measurement of the specific ionization loss, dE/dx, used for particle identification. Photons are detected using 7800 CsI crystals, which are also inside the magnet. Muons are identified using proportional counters placed at various depths in the steel return yoke of the magnet. The excellent efficiency and resolution of the CLEO-II detector for both charged particles and photons is used to suppress both continuum and combinatoric backgrounds.

Isolated showers with energies greater than 30 MeV in the central region of the detector, $|\cos\theta| < 0.71$, and greater than 50 MeV elsewhere, are defined to be photons. Pairs of photons with an invariant mass within 2σ of the π^0 mass are kinematically fitted with the mass constrained to the true π^0 mass. To further reduce combinatoric backgrounds, we require that the π^0 momentum be greater than 175 MeV/c, the shapes of the showers be consistent with those from photons, and that $|\cos\theta^*| < 0.97$, where θ^* is the angle between the direction of flight of the π^0 and the photons in the π^0 rest frame.

Tracks are required to pass track quality cuts based on the average hit residual and the impact parameters in both the $r-\phi$ and $r-z$ planes. We require that track momenta be greater than 175 MeV/c to match our charged track acceptance to that for neutral pions.

Pairs of tracks with vertices displaced from the primary interaction point are taken as K_s^0 candidates. The secondary vertex is required to be displaced from the primary interaction point by at least 5 mm for candidates with momenta greater than 1 GeV/c. This requirement is loosened to 2 mm for candidates with momenta less than 1 GeV/c to increase the efficiency when the decay distance is small. A momentum-dependent cut is also made on the χ^2 of the vertex fit. The $\pi^+\pi^-$ invariant mass is required to be within 12 MeV (2.5σ) of the nominal K^0 mass.

We form ϕ candidates from K^+K^- pairs with an invariant mass within 6.5 MeV (2.5σ) of the known ϕ mass. Similarly, ρ^+ or ρ^0 candidates are formed from $\pi^+\pi^0$ or $\pi^+\pi^-$ pairs with an invariant mass within 150 MeV (about 1Γ) of the known ρ mass, and $K^*(892)$ candidates are selected from $K\pi$ pairs with an invariant mass within 75 MeV (about 1.5Γ) of the known K^* masses. For the $K^*\pi$ searches, we only use the decay modes $K^{*0} \to K^+\pi^-$ and $K^{*+} \to K^+\pi^0$, whereas for the $K^*\phi$ searches we also include the decays $K^{*0} \to K^0\pi^0$ and $K^{*+} \to K^0\pi^+$.

Tracks are identified as kaons and/or pions if their specific ionization loss, dE/dx, is within 3σ of the expected value. Muons are rejected by requiring that the tracks not penetrate the steel absorber to a depth of five nuclear interaction lengths. Electrons are rejected based on dE/dx and the ratio of the track momentum to the associated shower energy in the CsI calorimeter. For certain classes of modes, candidates can have multiple interpretations under different particle hypotheses. In these cases we use a strict identification scheme where a track is positively identified as a kaon or a pion depending on which dE/dx hypothesis is more likely. To separate $K^+\pi^0$ from $\pi^+\pi^0$ strict identification is applied to the charged track. We also sort the modes $K^{*+}\pi^-$, $K^{*0}\pi^0$, $K^+\rho^-$, $\pi^+\rho^-$, and $\pi^0\rho^0$ (2 charged tracks plus a π^0) by requiring strict identification for both charged tracks. For the modes $K^{*0}\pi^+$, $K^+\rho^0$, and $\pi^+\rho^0$ (3 charged tracks) we require strict identification on the two like-sign tracks, while the unlike-sign track[1] is required to be consistent with the pion hypothesis within 2σ.

III. BACKGROUND SUPPRESSION

In general, $b \to c$ decays do not produce back-to-back particles with sufficient momentum to be a source of background to the rare decay modes under study. The only exception is for the three track modes $K^{*0}\pi^+$, $K^+\rho^0$, and $\pi^+\rho^0$ where the decay $B^+ \to \overline{D}^0\pi^+$, $\overline{D}^0 \to K^+\pi^-$ contributes to the background. Suppression of this background is discussed below. The dominant contribution to the background for all the decay modes comes from non-resonant (continuum) production of light quarks, $e^+e^- \to q\overline{q}$, $q = u, d, s, c$.

A. The ΔE – M_B plane

In the process $e^+e^- \to \Upsilon(4S) \to B\overline{B}$, the B mesons are produced with momenta of $\approx$ 300 MeV/c and with the same energy as the colliding $e^\pm$ beams, E_{beam}. We define the variable $\Delta E = E_{candidate} - E_{beam}$ to make use of this constraint. For Monte Carlo signal events, this variable has a Gaussian distribution centered near zero with a width of $15 - 50$ MeV, while for continuum background ΔE has a smooth linear shape over a broad range. In addition, ΔE provides information which helps to separate modes with kaons from modes with pions. For example, $K^+\pi$ events misidentified as $\pi^+\pi$ events have ΔE centered at -42 MeV. A signal region is defined by $|\Delta E| < 2.0 - 2.5\sigma$, where σ is the rms resolution determined from Monte Carlo studies. For the modes $B \to K^{*+}\pi^-$, $\pi^\pm\rho^\mp$ and $K^+\rho^-$, $\sigma_{\Delta E}$ is a function of the helicity angle[2], since the energy resolution of a π^0 is strongly dependent on its momentum. The ΔE signal regions and resolutions for each mode are given in Table I.

The other kinematical variable used is the B mass. Again we use the fact that the B mesons are produced with the $e^\pm$ beam energy, and define the beam-constrained mass, $M_B = \sqrt{E_{beam}^2 - \vec{p}_{candidate}^{\,2}}$, where $\vec{p}_{candidate}$ is the vector sum of the momenta of the candidate daughters. The use of the beam energy, rather than the measured candidate energy, improves the resolution in the B mass by about an order of magnitude. Since the B mesons are produced nearly at rest, the resolution in the beam-constrained mass is dominated by the spread in beam energy and is thus nearly independent of the B decay mode. Studies of fully reconstructed B-meson decays to charm determined the resolution in M_B to be $\sigma = 2.64 \pm 0.20$ MeV, consistent with Monte Carlo results in the modes under consideration here.

---

[1]Charge-strangeness correlations do not allow the unlike-sign track to be a kaon.

[2]See section III C for a definition of helicity angle.

The signal region is defined as $|M_B - 5280| < 6 - 8$ MeV, depending on the decay mode under consideration, shown in Table I.

B. Event shape

Since B mesons from $\Upsilon(4S)$ decay are produced nearly at rest in the laboratory frame, the B decays are isotropic and the resulting event shape is rather spherical. Continuum background events naturally contain high momentum back-to-back particles in the two opposing light quark jets. The strategy used in this analysis is to remove the tracks and showers from the B candidate and then examine the properties of the rest of the event. This approach was adopted since, for two-body charmless decays of B mesons, the two decay products are produced nearly back-to-back with momenta of 2.0-2.6 GeV/c, which makes the overall event shape more jet-like. We find the thrust axis of the candidate particles and the thrust axis of the rest of the particles in the event, and define θ_{thrust} to be the angle between these two axes. For continuum events, the thrust axis of the candidate is highly correlated with the thrust axis of the remainder of the event; the thrust axes for $B\overline{B}$ events are uncorrelated. To suppress continuum background we require $|\cos\theta_{thrust}| < 0.7$. This cut removes $\sim 90\%$ of the continuum background with $\sim 65\%$ efficiency for signal events.

Additional information remains which can be used to suppress continuum background. This information is not readily extracted in a single kinematical variable, so a more refined technique is needed. We use a Fisher discriminant [9], $\mathcal{F} = \sum_i \alpha_i x_i$, which is a linear combination of input variables, x_i, with coefficients, α_i, chosen to maximize the separation between signal and background distributions of $\mathcal{F}$. Eleven input variables are used in the Fisher discriminant: $|\cos\theta_B|$, where θ_B is the angle between the B candidate momentum and the beam axis; $|\cos\theta_{candidate}|$, where $\theta_{candidate}$ is the angle between the candidate thrust axis and the beam axis; and nine variables that measure the momentum flow of showers and tracks from the rest of the event in nine angular bins, each of $10°$, centered around the candidate thrust axis. The distribution in $\cos\theta_B$ is flat for continuum whereas $B\overline{B}$ signal events have a $\sin^2\theta_B$ distribution; $\cos\theta_{candidate}$ is flat for signal and tends to peak towards $|\cos\theta_{candidate}| = 1$ for continuum background. Monte Carlo continuum and signal events in the mode $\pi^+\pi^-$ were used to determine the coefficients, α_i. The output distributions for both continuum and signal are Gaussian with a separation of $\sim 1.2 - 1.3\sigma$. This separation is only weakly dependent on the particular mode being investigated, as seen in Figure 2. Requiring $\mathcal{F} < 0.5$ reduces continuum backgrounds by a factor of 2 to 3, after requiring $|\cos\theta_{thrust}| < 0.7$. The efficiencies for signal events are $\sim 80\%$.

C. Helicity

For the modes $B \to K^*\pi, K\rho, \pi\rho$ and $K\phi$, the vector mesons are fully polarized, so we expect a helicity distribution of $\cos^2\theta_h$, where θ_h is defined as the angle between a daughter of the vector meson and the direction of flight of the B meson in the rest frame of the vector meson. Since the background helicity distributions are much flatter, we require $|\cos\theta_h| > 0.5$ for the modes $K^*\pi, K\rho$, and $\pi\rho$, and $|\cos\theta_h| > 0.4$ for the mode $K^+\phi$. Although the decay

$B^0 \to K^0\phi$ also has a $\cos^2\theta_h$ distribution, no helicity cut is made since the background is negligible.

D. D^0 veto

In order to prevent events from the decay $B^+ \to \overline{D}^0\pi^+$ (where $\overline{D}^0 \to K^+\pi^-$) from being misidentified as $B \to K^{*0}\pi^+$, $K^+\rho^0$, or $\pi^+\rho^0$, any candidate which can be interpreted as $B^+ \to \overline{D}^0\pi^+$, with a $K\pi$ invariant mass within 16 MeV (about 2σ) of the known D^0 mass, is not allowed to be interpreted as any other channel. We expect less than half an event background per mode from $B^+ \to \overline{D}^0\pi^+$ after this veto. The $\overline{D}^0\pi^+$ signal from vetoed events is used as a cross check of signal distributions and efficiencies.

IV. BACKGROUND ESTIMATION AND CALCULATION OF UPPER LIMITS

In order to estimate the remaining background, we look in a large sideband region in the ΔE *vs.* M_B plane. The expected background in the signal region is obtained by scaling the number of events seen in the sideband region. The scale factors are found using off-resonance data as well as continuum Monte Carlo. The sideband regions are listed in Table I. In order to increase the statistics for the off-resonance sample used in determining the scale factors we have loosened various cuts, such as event shape, particle ID, and resonance mass windows. Studies indicate that the shapes of the ΔE and M_B distributions, and hence the values of the scale factors, are not affected by loosening these cuts.

The reconstruction efficiencies were determined using events generated with a GEANT-based Monte Carlo simulation program [10]. Systematic uncertainties were determined using data wherever possible. The track quality cuts were studied by embedding μ pair events in generic hadronic events. Momentum resolution was measured directly using selected two-body decays of B mesons. The beam-constrained mass resolution was measured in data using many exclusive decay modes of B mesons. The π^0 quality cuts were studied in data. The Fisher discriminant efficiency was checked with $B \to D\pi$ decays. Some of the largest systematic errors common to all analyses presented come from the $|\cos\theta_{thrust}| < 0.7$ cut (6%) and the $\mathcal{F}$ cut (5%). For higher multiplicity modes the uncertainty in the track finding efficiency of 2% per track, the uncertainty in the π^0 efficiency of 7% per π^0, and the uncertainty in the K^0 efficiency of 8% per K^0 make substantial contributions as well. In the $B \to K^*\pi$, $K\rho$, $\pi\rho$ analysis, the simulation of the efficiency for the method which is used to sort the modes based on particle identification has a systematic error of 15%. The analysis efficiencies, with systematic errors, appear in Table II.

To calculate upper limits we use the procedure outlined in the Review of Particle Properties [11] for evaluation of upper limits in the presence of background. The background is negligible for the $K^0\pi^0$ and $X_s\phi$ modes, so it is ignored when calculating upper limits for all of these modes. To account for the uncertainties in the estimated continuum background and in the efficiencies, we reduce the background estimate by its error and we reduce the efficiency by its systematic error prior to calculating branching fraction upper limits. We assume equal production of charged and neutral B mesons.

V. RESULTS

Event yields, background scale factors, expected backgrounds, 90% confidence level upper limits on the branching fractions, and a range of theoretical predictions for these decays appear in Table III.

For the pseudoscalar-vector meson decays $K^*\pi$, $K\rho$, and $\pi\rho$, upper limits for B^+ modes are a factor of 2 to 5 lower than those previously published [12]. The upper limits for the B^0 modes have been improved by a factor of 7 to 16, or are first limits [12]. With the exception of the decay $B^0 \to \pi^\pm\rho^\mp$, for which our upper limit is comparable to theoretical expectations, these upper limits are still roughly an order of magnitude above theoretical predictions [13]. Figures 3 and 4 are projections onto the M_B axis, after applying all other cuts, for the B^0 and B^+ modes, respectively.

Upper limits on the decays $B \to X_s\phi$ are in the range 10^{-4} to 10^{-5}, a factor of 4 to 13 improvement over previously published limits [12]. Our limit on the decay $B^+ \to K^+\phi$ is comparable to some theoretical predictions [13]. Figures 5 and 6 are projections onto the M_B axis, after applying all other cuts, for the pseudoscalar-vector and vector-vector modes, respectively.

The upper limit for the decay $B^+ \to K^0\pi^+$ is comparable to the previously published limit [12]. There is no previously published limit for the decay $B^0 \to K^0\pi^0$. Theoretical expectations [13] are about an order of magnitude below these upper limits. Figure 7 shows projections onto the M_B axis, after applying all other cuts, for these modes.

The upper limit placed on the decay $B^+ \to \pi^+\pi^0$ is an order of magnitude improvement on previous results [12], and is comparable to some theoretical predictions [13]. There are no previously reported results for the decays $B^+ \to K^+\pi^0$ and $B^0 \to \pi^0\pi^0$. Figure 8 shows the M_B distributions for these modes.

VI. UPDATED RESULTS FOR $K^+\pi^-$, $\pi^+\pi^-$ MODES

Our previously published results for $B^0 \to K^+\pi^-$ and $B^0 \to \pi^+\pi^-$ [6] showed a significant signal in the sum of the two modes, but we were unable to measure branching fractions for either of the modes individually. Since publication, we have added 50% more data. We repeat the analysis, with emphasis on measurements of the branching fractions for the individual modes.

This analysis [6] uses cuts similar to those described above. A likelihood fit is used to extract the yields in each mode. This makes full use of the distributions in dE/dx and ΔE to separate the different particle hypotheses, and utilizes the shapes of the $\mathcal{F}$, ΔE, and M_B distributions to distinguish continuum background from signal. Updated results appear in Table IV and Figure 9.[3] We continue to quote upper limits since the signals for $K^+\pi^-$ and $\pi^+\pi^-$ are only 2.6σ and 2.8σ from zero, respectively. The significance of the combined result is 5.3σ statistical and 4.0σ including systematics.

---

[3]Cuts on ΔE and $\mathcal{F}$, which have an efficiency of $\sim 50\%$ relative to the likelihood analysis, are made to reduce the background prior to producing this mass plot.

VII. CONCLUSIONS

We have presented new upper limits on the branching fractions for a variety of charmless hadronic decays of B mesons, as well as updated results for the decays $B^0 \to K^+\pi^-$ and $B^0 \to \pi^+\pi^-$. These decays probe both $b \to sg$ and $b \to u$ transitions. These results are significant improvements over those previously published. Our sensitivity is at the level of theoretical predictions for the modes $\pi^+\pi^-$, $K^+\pi^-$, $\pi^+\pi^0$, $\pi^\pm\rho^\mp$, $K^+\phi$, and $K^{*0}\phi$.

VIII. ACKNOWLEDGEMENTS

We gratefully acknowledge the effort of the CESR staff in providing us with excellent luminosity and running conditions. J.P.A. and P.S.D. thank the PYI program of the NSF, I.P.J.S. thanks the YI program of the NSF, G.E. thanks the Heisenberg Foundation, K.K.G., I.P.J.S., and T.S. thank the TNRLC, K.K.G., H.N.N., J.D.R., T.S. and H.Y. thank the OJI program of DOE and P.R. thanks the A.P. Sloan Foundation for support. This work was supported by the National Science Foundation, the U.S. Dept. of Energy and the Natural Sciences and Engineering Research Council of Canada.

REFERENCES

[1] B Physics Task Force, "Physics and Detector of Asymmetric B Factory at KEK", KEK report 90-23 (1991); CESR-B Physics Working Group (K. Lingel, *et al.*), "Physics Rationale for a B Factory", Cornell Report CLNS 91-1043 (1991); "The Physics Program of a High-Luminosity Asymmetric B Factory at SLAC" SLAC Report SLAC-353 (1989).

[2] See for example S. Erhan in "The Proceedings of the Workshop on Beauty '93" (ed. P. E. Schlein), Liblice Castle, Melink, Czech Republic, Nucl. Instr. and Meth. A **333**, 213 (1993), and references therein.

[3] J.P. Silva and L. Wolfenstein, Phys. Rev. D **49**, 1151 (1994); M. Gronau, Phys. Rev. Lett. **63**, 1451 (1989).

[4] M. Gronau and D. London, Phys. Rev. Lett. **65**, 3381 (1990).

[5] M. Gronau, J. L. Rosner, and D. London, Phys. Rev. Lett. **73**, 21 (1994);

[6] M. Battle *et al.* (CLEO), Phys. Rev. Lett. **71**, 3922 (1993).

[7] R. Ammar *et al.* (CLEO), Phys. Rev. Lett. **71**, 674 (1993).

[8] Y. Kubota *et al.* (CLEO), Nucl. Instr. Methods A**320**, 66 (1992).

[9] M. G. Kendall and A. Stuart, *The Advanced Theory of Statistics*, Second Edition, (Hafner, New York, 1968) Vol. III, §44.5*ff*; R. A. Fisher, Ann. Eugen. **7** 179 (1936).

[10] We thank the CERN computer staff for maintaining the GEANT detector simulation (version 3.14, CERN DD/EE/84-1, R. Brun *et al.*) code.

[11] Particle Data Group, "Review of Particle Properties," Phys. Rev. D **45**, S1 (1992).

[12] H. Albrecht *et al.* (ARGUS), Phys. Lett. B**254**, 288 (1991); H. Albrecht *et al.* (ARGUS), Phys. Lett. B**241**, 278 (1990); P. Avery *et al.* (CLEO), Phys. Lett. B**223**, 470 (1989); D. Bortoletto *et al.* (CLEO), Phys. Rev. Lett. **62**, 2436 (1989); C. Bebek *et al.* (CLEO), Phys. Rev. D**36**, 1289 (1987).

[13] A. Deandrea, N. Di Bartolomeo, R. Gatto, F. Feruglio, and G. Nardulli, Phys. Lett. B**320**, 170 (1994); N. G. Deshpande and Xiao-Gang He, OITS-538 (1994); A. Deandrea, N. Di Bartolomeo, R. Gatto, and G. Nardulli, Phys. Lett. B**318**, 549 (1993); A.J. Davies, T. Hayashi, M. Matsuda, and M. Tanimoto, AUE-02-93; L. L. Chau, H-Y Cheng, W.K. Sze, H. Yao, and B. Tseng, Phys. Rev. D**43**, 2176 (1991); N. G. Deshpande and J. Trampetic, Phys. Rev. D**41**, 895 (1990); M. Bauer, B. Stech, and M. Wirbel, Z. Phys. C**43**, 103 (1987).

TABLE I. Resolutions on ΔE, the signal regions in ΔE and $\Delta M_B = M_B - 5280$ MeV, and the sideband regions in ΔE and M_B. For the decays $B \to X_s \phi$, particles in parentheses indicate a $K^*(892)$ decaying to those particles.

		Signal Region		Sideband Region	
Mode	$\sigma_{\Delta E}$ (MeV)	$\|\Delta E\|$ (Mev)	$\|\Delta M_B\|$ (MeV)	$\|\Delta E\|$ (MeV)	M_B (MeV)
$\pi^0\pi^0$	68	$-170 < \Delta E < 100$	< 8.0	< 300	$5200 < M_B < 5270$
$\pi^\pm\rho^\mp$	25-45	$< 2\sigma^\ddagger$	< 6.0	< 200	$5200 < M_B < 5270$
$\pi^0\rho^0$	45	< 90	< 6.0	< 200	$5200 < M_B < 5270$
$\pi^+\pi^0$	49	$-110 < \Delta E < 90$	< 8.0	< 300	$5200 < M_B < 5270$
$\pi^+\rho^0$	25	< 50	< 6.0	< 200	$5200 < M_B < 5270$
$K^0\pi^0$	44	$-105 < \Delta E < 75$	< 6.5	< 200	$5200 < M_B < 5290^\dagger$
$K^{*+}\pi^-$	25-45	$< 2\sigma^\ddagger$	< 6.0	< 200	$5200 < M_B < 5270$
$K^{*0}\pi^0$	45	< 90	< 6.0	< 200	$5200 < M_B < 5270$
$K^+\rho^-$	25-45	$< 2\sigma^\ddagger$	< 6.0	< 200	$5200 < M_B < 5270$
$K^0\phi$	18	< 44	< 6.5	< 200	$5200 < M_B < 5290^\dagger$
$(K^+\pi^-)\phi$	20	< 50	< 6.5	< 200	$5200 < M_B < 5290^\dagger$
$(K^0\pi^0)\phi$	24	< 59	< 6.5	< 200	$5200 < M_B < 5290^\dagger$
$\phi\phi$	16	< 39	< 6.5	< 200	$5200 < M_B < 5290^\dagger$
$K^+\pi^0$	49	$-110 < \Delta E < 90$	< 8.0	< 300	$5200 < M_B < 5270$
$K^0\pi^+$	27	< 65	< 6.5	< 200	$5200 < M_B < 5290^\dagger$
$K^{*0}\pi^+$	25	< 50	< 6.0	< 200	$5200 < M_B < 5270$
$K^+\rho^0$	25	< 50	< 6.0	< 200	$5200 < M_B < 5270$
$K^+\phi$	23	< 57	< 6.5	< 200	$5200 < M_B < 5290^\dagger$
$(K^+\pi^0)\phi$	23	< 58	< 6.5	< 200	$5200 < M_B < 5290^\dagger$
$(K^0\pi^+)\phi$	17	< 43	< 6.5	< 200	$5200 < M_B < 5290^\dagger$

† Excluding the signal region

‡ The ΔE resolution and cut are functions of helicity.

TABLE II. Reconstruction efficiencies and daughter branching ratios. For the decays $B \to X_s \phi$, particles in parentheses indicate a $K^*(892)$ decaying to those particles.

Mode	Reconstruction Efficiency (%)	BR(daughters)	Eff. $\times$ BR (%)
$\pi^0\pi^0$	18.4 ± 2.8	0.976	18.0 ± 2.7
$\pi^\pm\rho^\mp$	5.1 ± 1.1	0.988	5.2 ± 1.0
$\pi^0\rho^0$	6.1 ± 1.2	0.988	6.4 ± 1.2
$\pi^+\pi^0$	18.5 ± 2.7	0.988	18.3 ± 2.7
$\pi^+\rho^0$	7.4 ± 1.5	1.0	7.4 ± 1.5
$K^0\pi^0$	13.4 ± 2.0	0.339	4.5 ± 0.7
$K^{*+}\pi^-$	4.3 ± 0.9	0.333	1.5 ± 0.2
$K^{*0}\pi^0$	5.4 ± 1.1	0.659	3.7 ± 0.7
$K^+\rho^-$	5.4 ± 1.1	0.988	5.7 ± 1.1
$K^0\phi$	10.9 ± 1.6	0.168	2.0 ± 0.3
$(K^+\pi^-)\phi$	16.9 ± 3.4	0.327	5.3 ± 1.0
$(K^0\pi^0)\phi$	5.6 ± 1.1	0.054	0.3 ± 0.1
$\phi\phi$	11.0 ± 1.7	0.241	2.6 ± 0.4
$K^+\pi^0$	18.3 ± 2.7	0.988	18.1 ± 2.7
$K^0\pi^+$	20.7 ± 3.1	0.343	7.1 ± 1.1
$K^{*0}\pi^+$	7.0 ± 1.4	0.667	4.7 ± 0.9
$K^+\rho^0$	7.1 ± 1.4	1.0	7.1 ± 1.4
$K^+\phi$	17.9 ± 2.7	0.491	8.6 ± 1.3
$(K^+\pi^0)\phi$	7.9 ± 1.6	0.160	1.5 ± 0.3
$(K^0\pi^+)\phi$	9.3 ± 1.9	0.112	1.0 ± 0.2

TABLE III. Event yields, sideband scale factors, estimated backgrounds in the signal region, upper limits on the branching ratios, and theoretical predictions. Upper limits are at the 90% confidence level. For the decays $B \to X_s \phi$, particles in parentheses indicate a $K^*(892)$ decaying to those particles.

Mode	Event Yields signal	sideband	Scale Factor (%)	Est. Bkgr.	Upper Limit on BR (10^{-5})	Theory [13] (10^{-5})
$\pi^0\pi^0$	1	20	8.7 ± 0.4	1.7 ± 0.4	1.0	0.03-0.10
$\pi^\pm\rho^\mp$	6	74	3.3 ± 0.7	2.4 ± 0.6	9.5	1.9-8.8
$\pi^0\rho^0$	1	35	4.2 ± 1.2	1.5 ± 0.5	2.9	0.07-0.23
$\pi^+\pi^0$	8	127	4.6 ± 0.2	5.8 ± 0.6	2.3	0.6-2.1
$\pi^+\rho^0$	3	77	2.4 ± 0.4	1.8 ± 0.3	4.1	0.0-1.4
$K^0\pi^0$	2	7			6.3	0.5-0.8
$K^{*+}\pi^-$	3	22	2.8 ± 0.8	0.6 ± 0.2	23.8	0.1-1.9
$K^{*0}\pi^0$	0	11	8.0 ± 1.7	0.9 ± 0.3	3.5	0.3-0.5
$K^+\rho^-$	2	57	3.1 ± 0.6	1.7 ± 0.4	4.3	0.0-0.2
$K^0\phi$	1	1			10.7	0.1-1.3
$(K^+\pi^-)\phi$	1	19				
$(K^0\pi^0)\phi$	0	0				
$K^{*0}\phi$ (combined)	1	19			3.9	0.0-3.1
$\phi\phi$	0	1			4.8	–
$K^+\pi^0$	10	102	4.9 ± 0.2	5.0 ± 0.5	3.2	0.3-1.3
$K^0\pi^+$	6	61	3.3 ± 0.7	2.0 ± 0.5	6.8	1.1-1.2
$K^{*0}\pi^+$	2	30	2.0 ± 0.5	0.6 ± 0.2	6.0	0.6-0.9
$K^+\rho^0$	1	52	2.1 ± 0.4	1.1 ± 0.2	2.6	0.01-0.06
$K^+\phi$	0	13			1.4	0.1-1.5
$(K^+\pi^0)\phi$	0	10				
$(K^0\pi^+)\phi$	1	2				
$K^{*+}\phi$ (combined)	1	12			9.0	0.0-3.1

TABLE IV. Updated results for $B^0 \to K^+\pi^-$, $B^0 \to \pi^+\pi^-$, and $B^0 \to K^+K^-$. Upper limits are at the 90% confidence level.

Mode	Event Yield	BR (10^{-5})	Theoretical Predictions (10^{-5}) [13]
$\pi^+\pi^-$	$8.5^{+4.9}_{-4.0}$	< 2.2	1.0-2.6
$K^+\pi^-$	$7.1^{+4.2}_{-3.4}$	< 1.9	1.0-2.0
K^+K^-	$0.0^{+1.6}_{-0.0}$	< 0.7	–
$\pi^+\pi^- + K^+\pi^-$	$15.7^{+5.3}_{-4.5}$	$1.8^{+0.6}_{-0.5} \pm 0.2$	

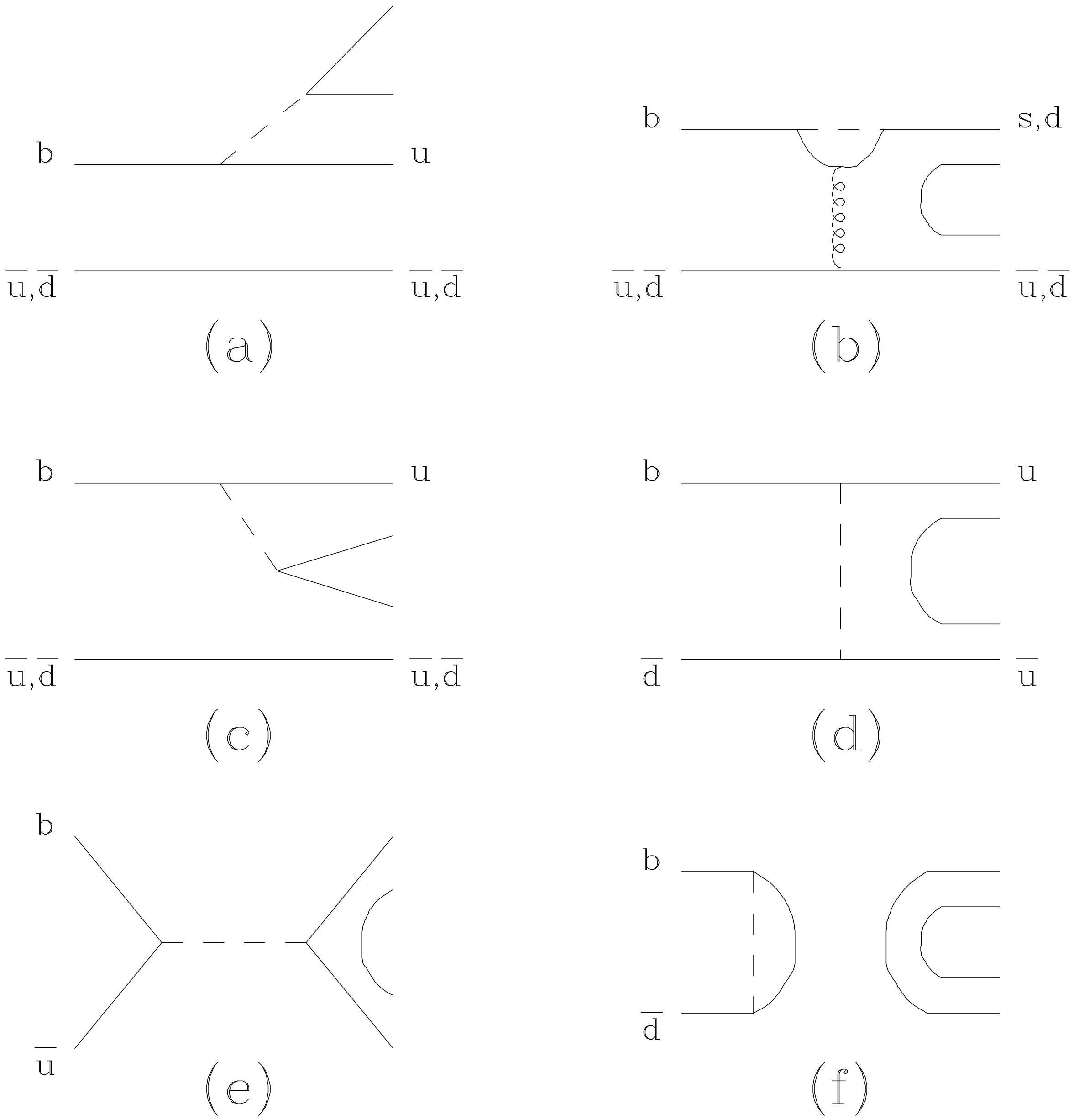

FIG. 1. Feynman diagrams: (a) external W emission, (b) loop or gluonic penguin, (c) internal W, (d) W exchange, (e) annihilation, and (f) vertical W loop.

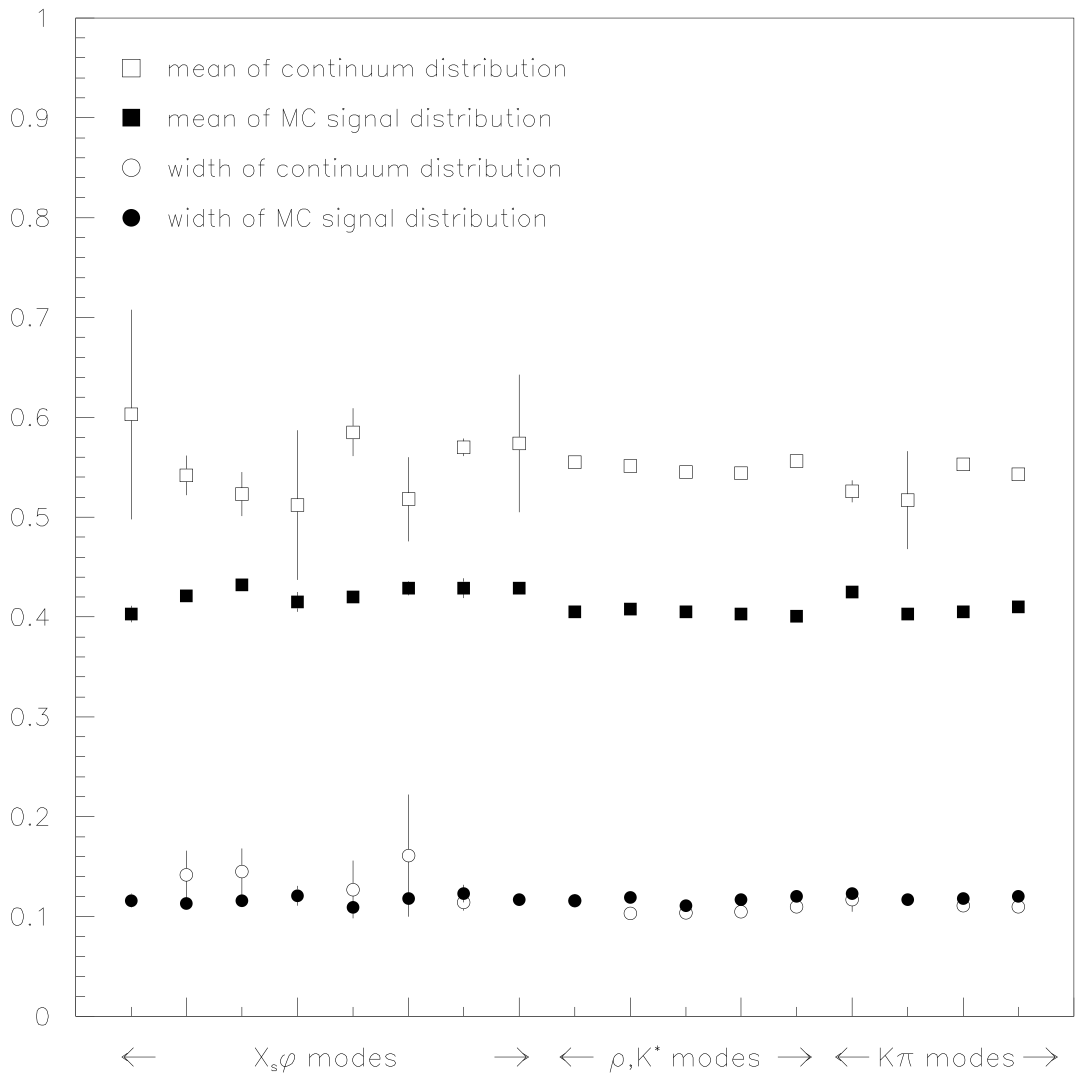

FIG. 2. Mean and width of $\mathcal{F}$ distributions for signal Monte Carlo and continuum background data for the modes discussed in this paper. Note the remarkable stability of the results over a very broad variety of decay modes.

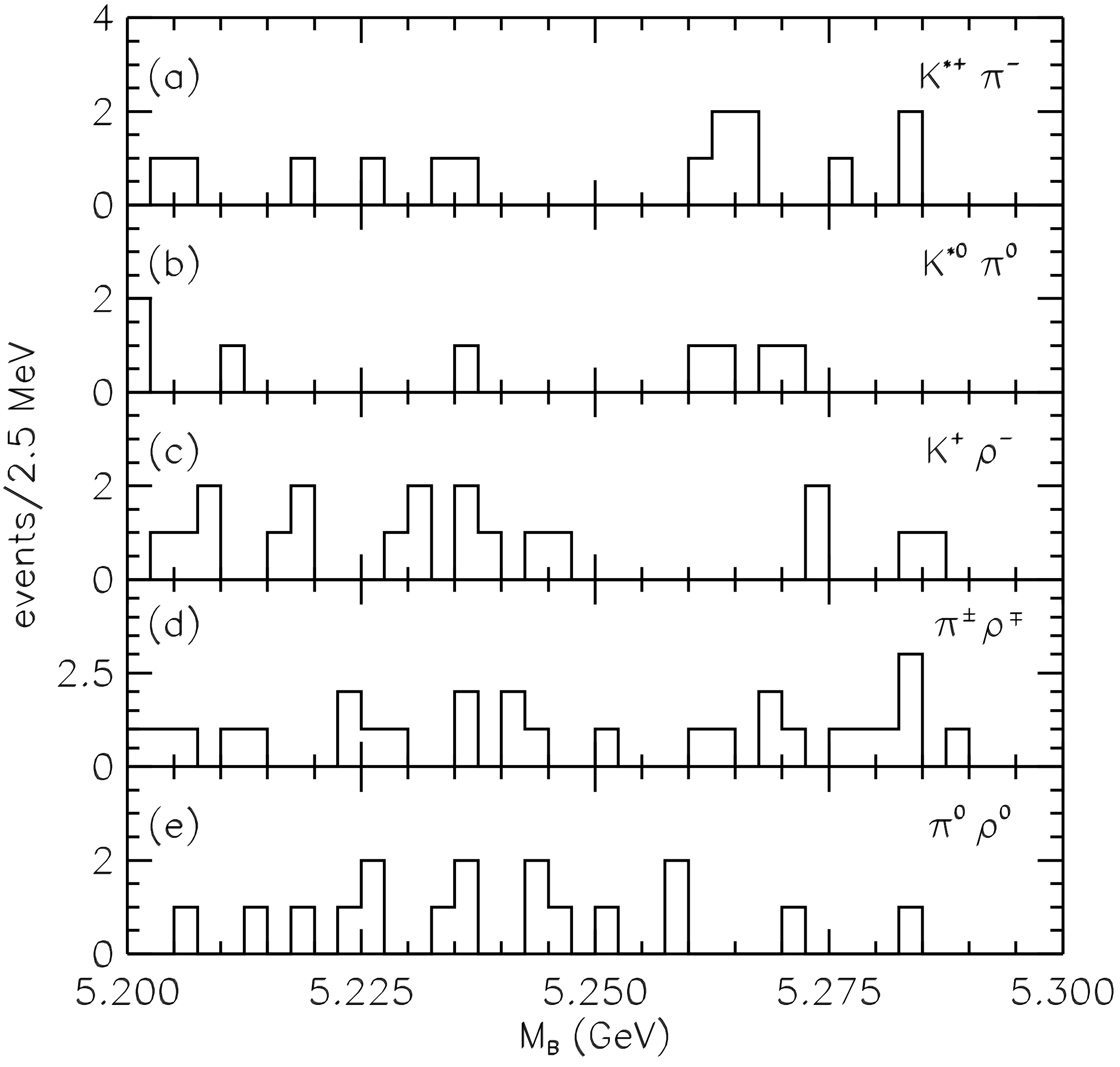

FIG. 3. Beam-constrained mass for (a) $B^0 \to K^{*+}\pi^-$, (b) $B^0 \to K^{*0}\pi^0$, (c) $B^0 \to K^+\rho^-$, (d) $B^0 \to \pi^\pm\rho^\mp$, and (e) $B^0 \to \pi^0\rho^0$ candidates.

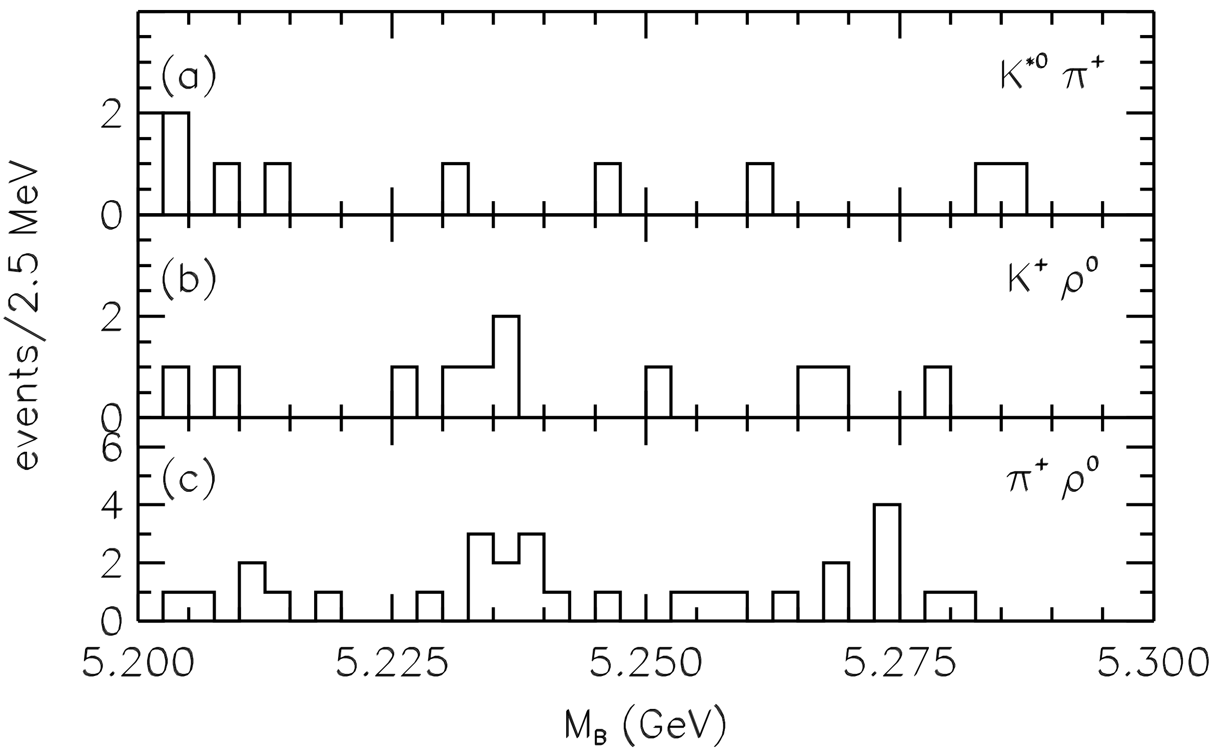

FIG. 4. Beam-constrained mass for (a) $B^+ \to K^{*0}\pi^+$, (b) $B^+ \to K^+\rho^0$, and (c) $B^+ \to \pi^+\rho^0$ candidates.

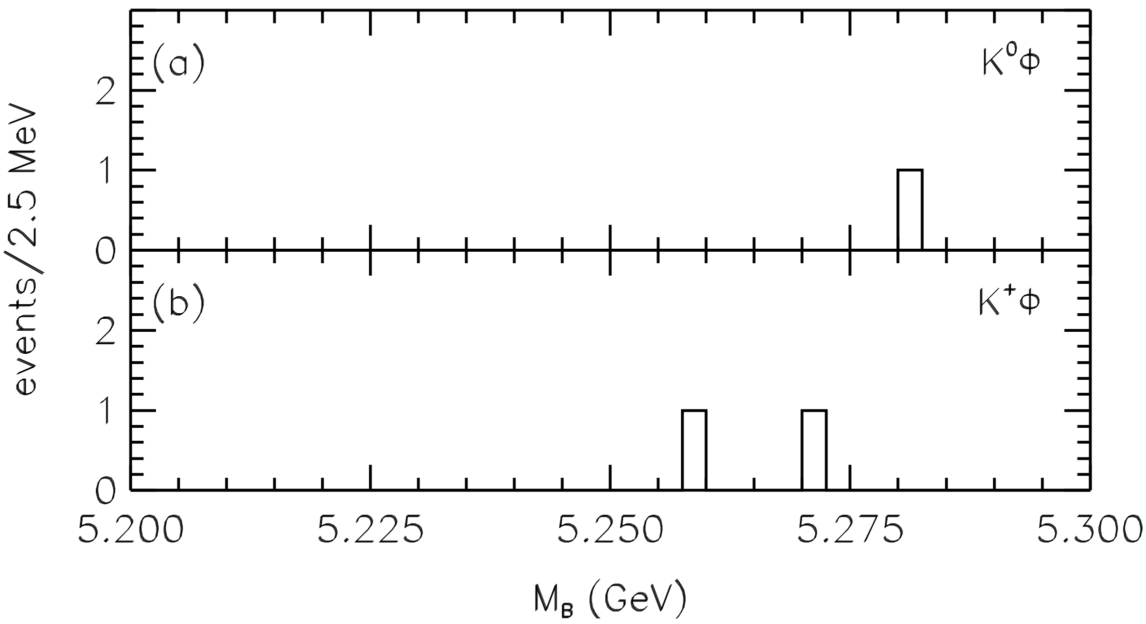

FIG. 5. Beam-constrained mass for (a) $B^0 \to K^0\phi$ and (b) $B^+ \to K^+\phi$ candidates.

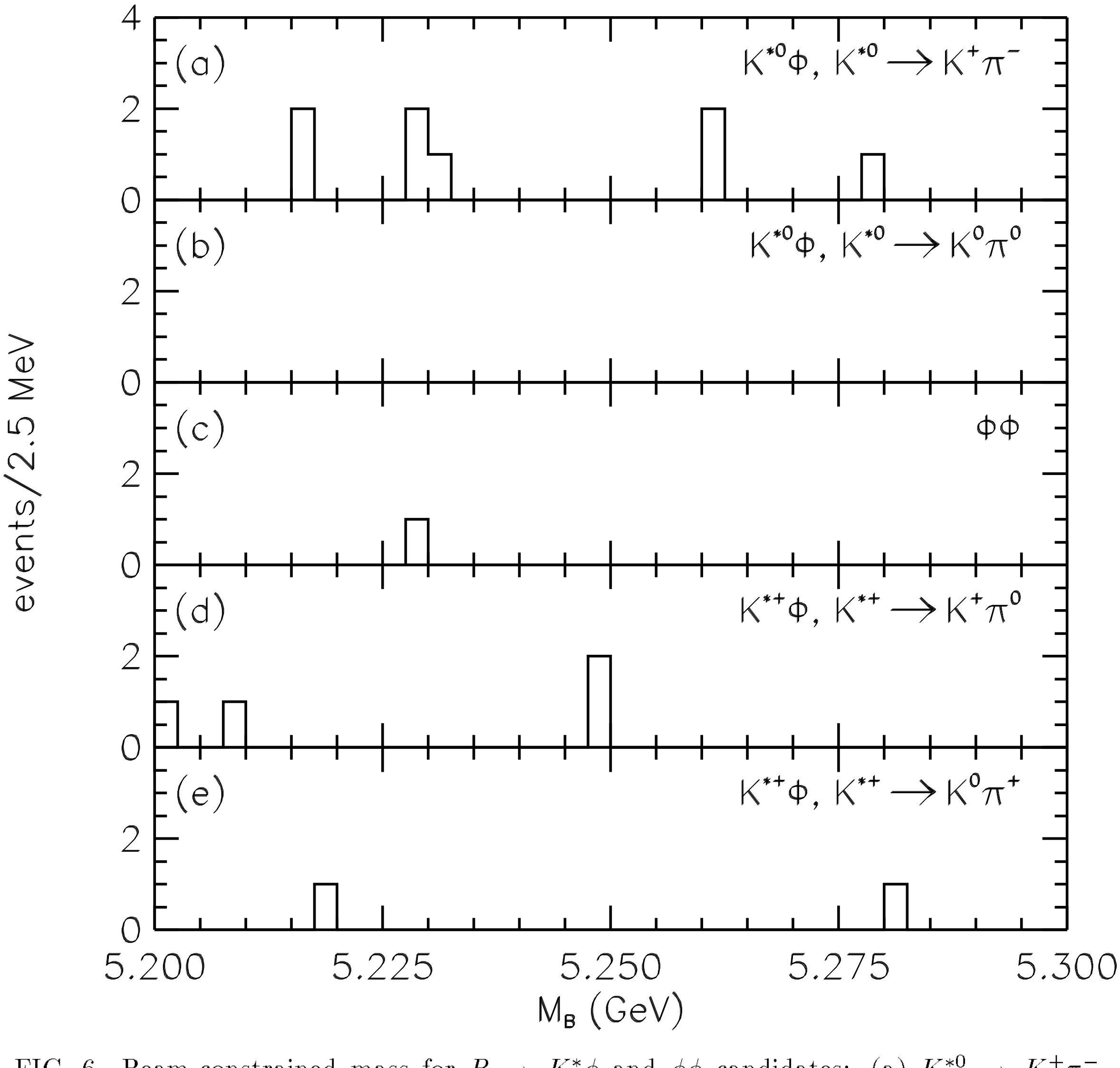

FIG. 6. Beam-constrained mass for $B \to K^*\phi$ and $\phi\phi$ candidates: (a) $K^{*0} \to K^+\pi^-$, (b) $K^{*0} \to K^0\pi^0$, (c) $\phi\phi$, (d) $K^{*+} \to K^+\pi^0$, and (e) $K^{*+} \to K^0\pi^+$.

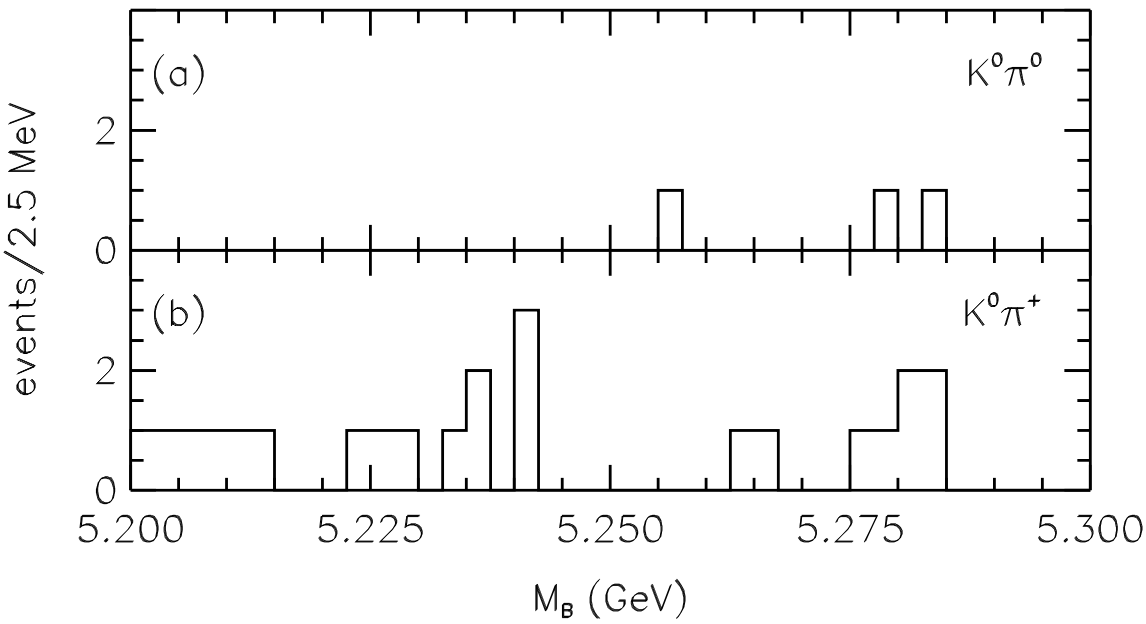

FIG. 7. Beam-constrained mass for (a) $B^0 \to K^0\pi^0$ and (b) $B^+ \to K^0\pi^+$ candidates.

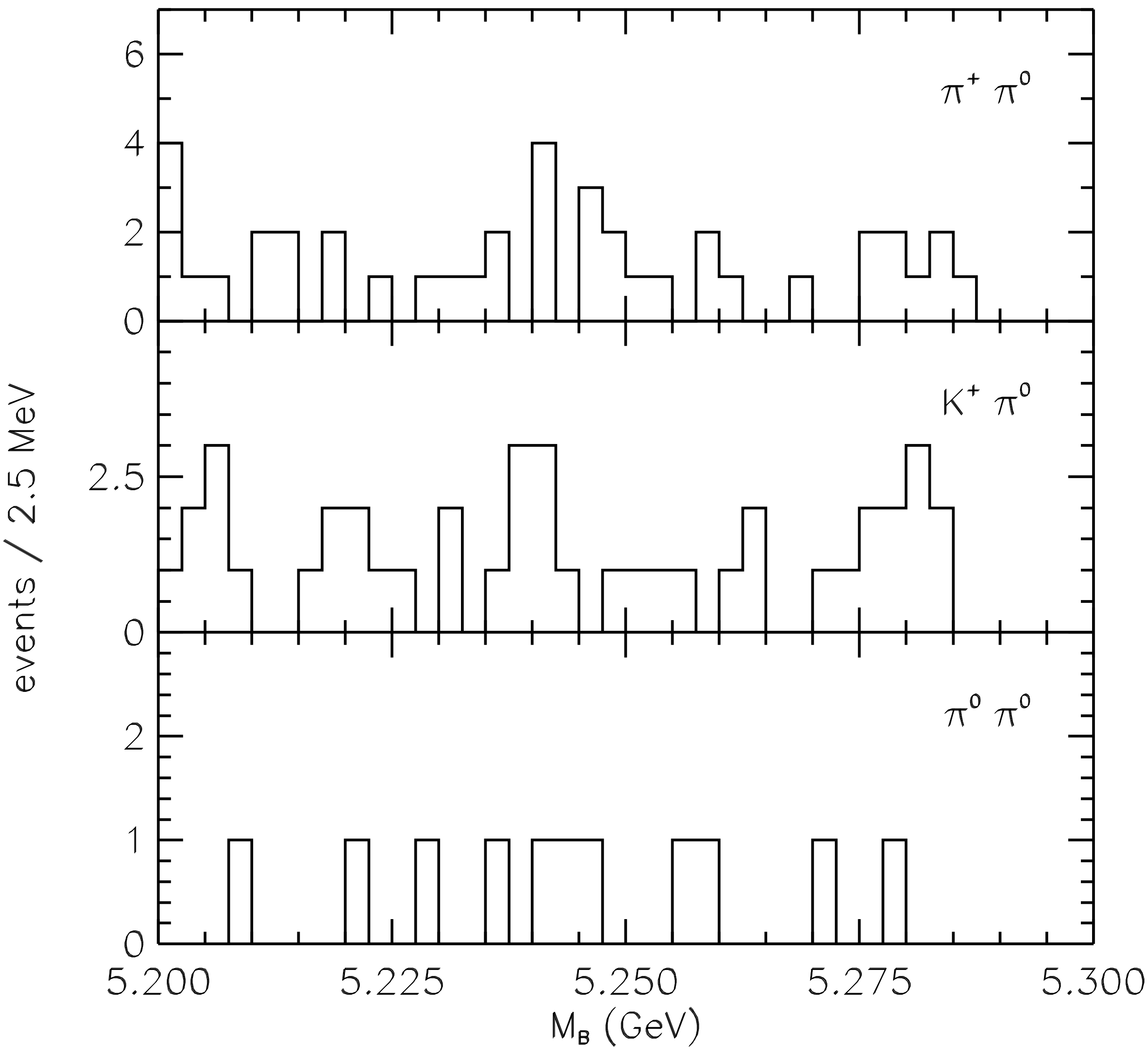

FIG. 8. Beam-constrained mass for (a) $B^+ \to \pi^+\pi^0$, (b) $B^+ \to K^+\pi^0$, and (c) $B^0 \to \pi^0\pi^0$.

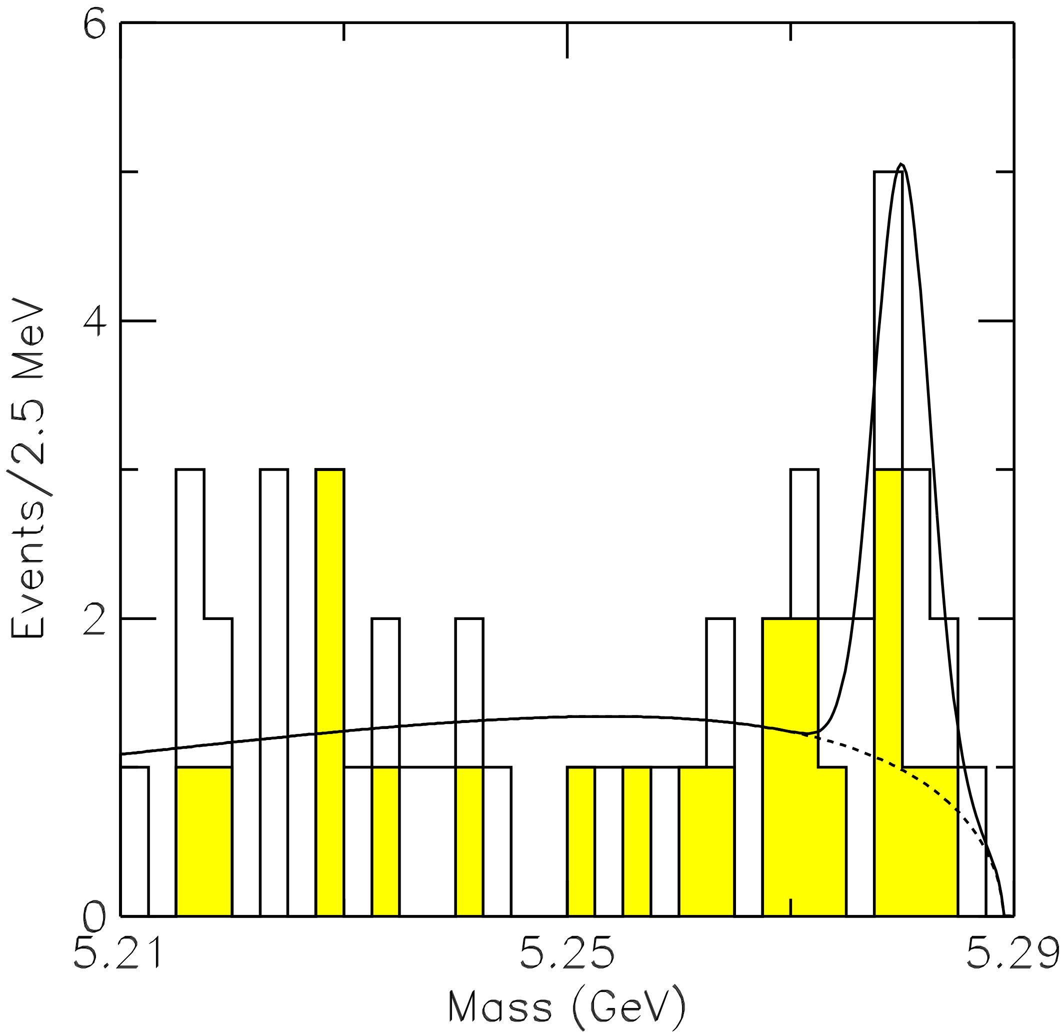

FIG. 9. The projection onto M_B of the sum of $\pi^+\pi^-$ (shaded) and $K^+\pi^-$ (unshaded) events, after cutting on ΔE and $\mathcal{F}$. The curve is the projection of the maximum likelihood fit.